Effects of different rock density profiles on magma ascent and on the statistical distributions of simulated eruptions

E. Piegari[1], R. Di Maio[1] and R. Scandone[2]

[1] *Dipartimento di Scienze della Terra, Università "Federico II", Napoli, Italy*
[2] *Dipartimento di Fisica "E. Amaldi", Università di Roma Tre, Roma Italy*

ABSTRACT   The structure of a volcanic edifice depends on composition, volume of erupted magma, and mechanism of eruption. In particular, pressure variations with depth due to density variations of the volcanic rocks are crucial for magma degassing processes as well as buoyancy mechanisms. In this paper, we analyze the effects of three different pressure profiles with depth on the probability of occurrence of simulated eruptive events. We describe the dynamics of magma ascent by means of a time dependent Self-Organized Criticality field, which controls the opening of crack networks through which discrete magma batches are allowed to rise. We find a characteristic power-law behavior for the number of eruptions with erupted volume in all considered cases. As concerns the probability of occurrence of an eruptive event with a given percentage of gas losses, we find that extreme events, i.e., events with the lowest percentage of gas losses, are more likely to occur if a step function is used to describe the relationship between rock density and depth.

1. Introduction

The rock density increases with depth in the Earth, as pressures rise. However, changes in density with increasing depth may also be influenced by other factors, such as lithology, porosity, presence of fractures. Usually, rock density is measured either by laboratory experiments on core samples or by in-situ geophysical measurements. Since deep rock samples are not available, gravimetric and/or seismic geophysical methods are generally used to obtain information on density of the Earth's internal structure (Gardner *et al*., 1974; Rymer and Brown, 1986). In particular, volcanoes are generated only when structural conditions and particular rock density distributions occur, allowing magma rising. Moreover, the density profile of a volcanic edifice strongly influences the magma dynamics since it can affect the discharge rate and degassing processes. In order to investigate the effect of rock density profiles on explosivity of eruptions, we performed numerical simulations of magma ascent by considering three different density-depth functions.

In a different way from traditional approaches, which describe the magma ascent by means of solutions of partial differential equations of fluid mechanics, we use a statistical approach aimed at reproducing the eruptive activity of a volcano. We do not assume a conduit of assigned geometry, but start from a transport region where a time-dependent Self-Organized field controls

the opening of crack networks through which discrete magma batches are allowed to rise. During the ascent, magma loses gas in a way that depends on the rock density distributions. Therefore, the choice of an appropriate density-depth function is essential for the computation of probability distributions of eruptive events with a given degree of explosivity.

2. The statistical model

Contrary to traditional approaches, which assume the magma ascent through conduits of fixed geometry (Papale, 1999; Legros *et al.*, 2000), we model the magma rising as an infiltration process through rock fractures (Scandone *et al.*, 2007; Piegari *et al.*, 2008, 2011), whose location and sizes are controlled by Self Organized Criticality (SOC: Bak, 1996). To this aim, we approximate the vertical section of a volcano by means of a two-dimensional grid whose square cells are characterized by the values of two interacting fields: the field that controls the opening of fractures in the surrounding rock, e, and the field of local presence of magma, n.

2.1. Modeling fracturing mechanism

Fractures in the rocks open in response to triggering mechanisms of different origins, such as earthquakes, local regional stress. In our model (Piegari *et al.*, 2008, 2011), we do not specify the cause of fracturing, but describe it by means of a SOC field. We start from an initial non fractured configuration, i.e., we attribute to each cell i a uniformly distributed random value of e_i, with $0 < e_i < 1$ $\forall i$, which we expect to capture the heterogeneity of the stress values in the rock (Piegari *et al.*, 2006). Since e represents the ratio of driving forces to resisting forces, a cell becomes fractured only if e reaches the threshold value $e_{th} = 1$. When a cell fractures, it relaxes and transfers its stress instability to the four nearest neighbors cells that, in their turn, can fracture and transfer their instability to nearest neighbors and so on. The fracturing process stops when all cells return below the threshold value e_{th}. In the simulations, we consider the isotropic case for stress redistribution, which means that the four transfer parameters are equal to a constant value f, and the non-conservative limit, $4f < 1$, to capture the dissipative nature of real systems (see Piegari *et al.*, 2008).

2.2. Modeling magma infiltration

To describe the local presence of magma in the volcanic edifice, we attribute to each cell of the grid a value of the field n. If a cell is empty, the corresponding value of n is 0. If a cell is filled with magma, the corresponding value of n ranges between 1 and $1 - n_{loss}$, where n_{loss} is the percentage of gas loss (see section 2.3). At the bottom line of the grid, we locate the magma reservoir, which is constituted by $L/4$ cells filled with magma ($n = 1$), where L is the linear dimension of the system. When a cell adjacent to the magma reservoir becomes fractured, magma is allowed to ascend and move through all connected fractured cells. If fractured cells are connected to the surface, magma is discharged and an eruption occurs. If fractured cells are not connected to the surface, magma stops within the transport region and loses gas as described below. In Figs. 1 and 2, two snapshots show typical configurations of the system corresponding to a big and small eruptive event, respectively.

It is worthwhile noting that to describe the formation of a central conduit, we assume an axial
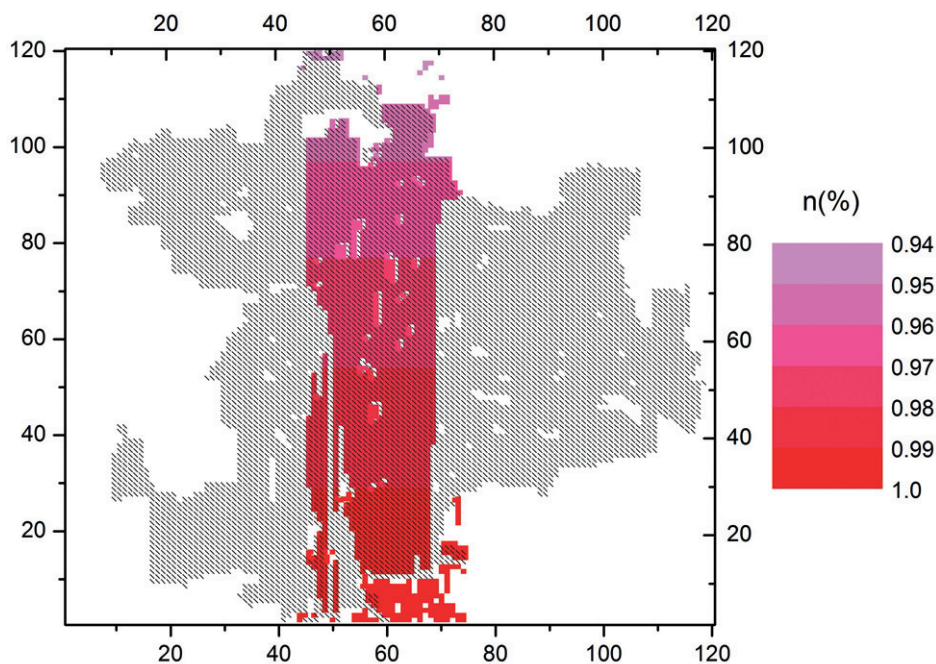
Fig. 1 - Snapshot of a large synthetic eruptive event involving about 2000 cells and connecting the reservoir to the surface. Since a path of fractures connected to the surface is opened, magma stored in the system is discharged. White cells represent non-fractured rocks, shaded cells represent fractured cells, colored cells correspond to cells that contain magma. Color scale reports magma degassing: red cells are rich of gas, magenta cells are completely degassed.

symmetry in the dynamical rules of the field *n*. In other words, we impose that from the half of the height of the simulated volcanic edifice, horizontal movements of magma are allowed only if they are towards the central axis of the grid.

2.3. Modeling magma degassing

The amount of gas in a magma is a key ingredient for explosivity. At high lithostatic pressure, gas is dissolved in the liquid, but it starts to exsolve when pressure is decreased. To simplify the description of degassing processes, we take into account only the water content of the magma, which we consider at the saturation pressure in the magma reservoir. Therefore, as magma rises, it loses an amount of gas, which depends on pressure. We use the relationship between the dissolved water concentration, n_d, and lithostatic pressure, p, for basalt (Scandone and Giacomelli, 1998)

$$n_d = 0.0215 p^{0.7}. \tag{1}$$

The lithostatic pressure is the pressure imposed on a layer of soil or rock by the weight of overlying material. At a depth *z*, it is given by
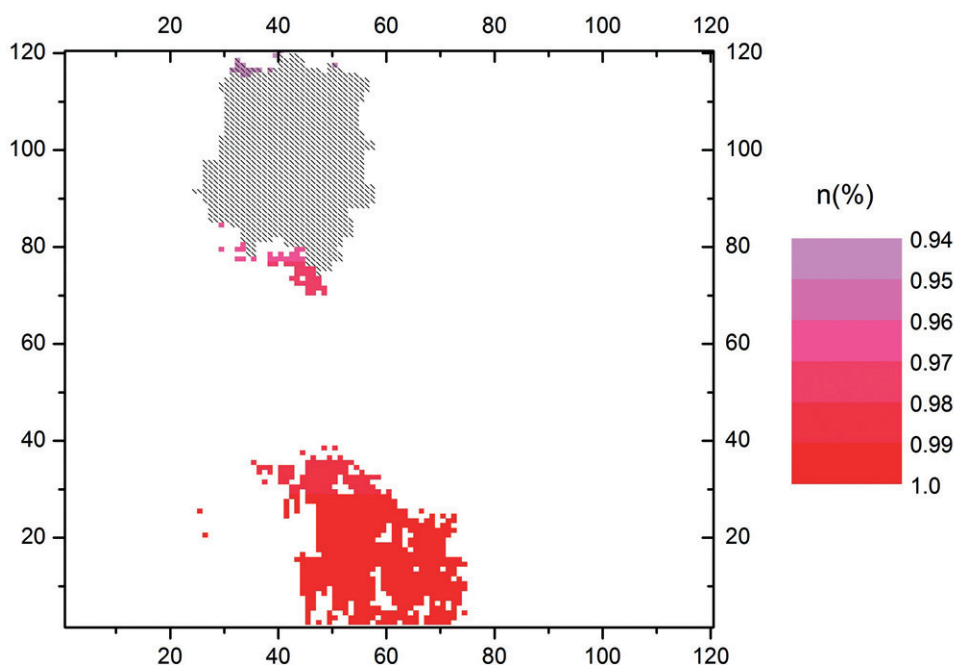
Fig. 2 - Snapshot of a synthetic eruptive event involving 14 cells. White cells represent non-fractured rocks, shaded cells represent fractured cells, colored cells correspond to cells that contain magma. Color scale reports magma degassing: red cells are rich in gas, magenta cells are completely degassed.

$$p = p_0 + g \int_0^z \rho(z)dz \qquad\qquad (2)$$

where $\rho(z)$ is the density of the overlying rock at depth z, g is the acceleration due to gravity, and p_0 is the pressure at the surface. In the following, we study statistical distributions of simulated eruptive events by using the three different rock density profiles shown in Fig. 3. In the first case, we assume a constant rock density $\rho_1 = 2700$ kg/m^3; in the second case, we approximate the rock density to a step function $\rho_2(z)$, while in the third case, we consider the rock density as a linear function of the depth $\rho_3(z)=a+bz$, where the constants a and b are found by imposing that the rock density value is 3000 kg/m^3 at the bottom of the volcanic edifice ($z = 12$ km) and 2200 kg/m^3 at the surface ($z = 0$).

Substituting Eq. (2) in Eq. (1), we calculate the changes of the dissolved water concentration with the depth. To estimate the percentage of gas loss, n_{loss}, we assume that the exsolved water, n_e, is completely lost, $n_{loss}= n_e$, and calculate the exsolved water by the following equation (Sparks, 1978; Wilson and Head, 1981):
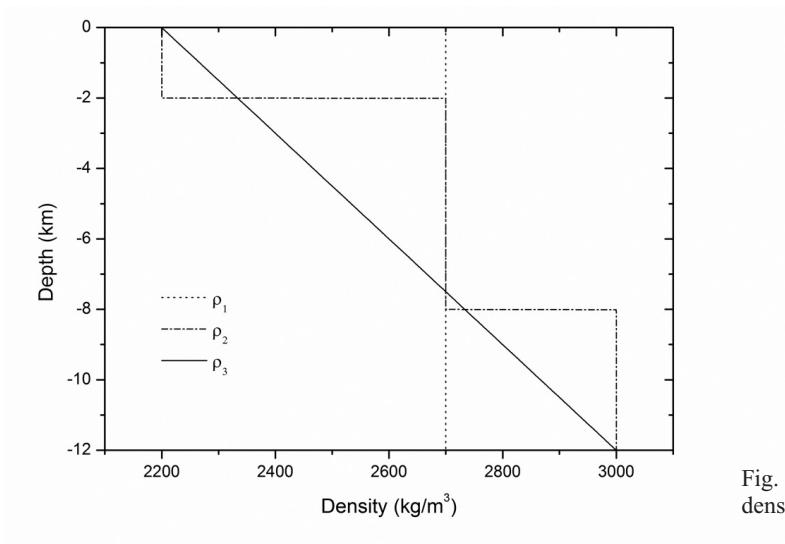
Fig. 3 - The analyzed three different rock density-depth functions.
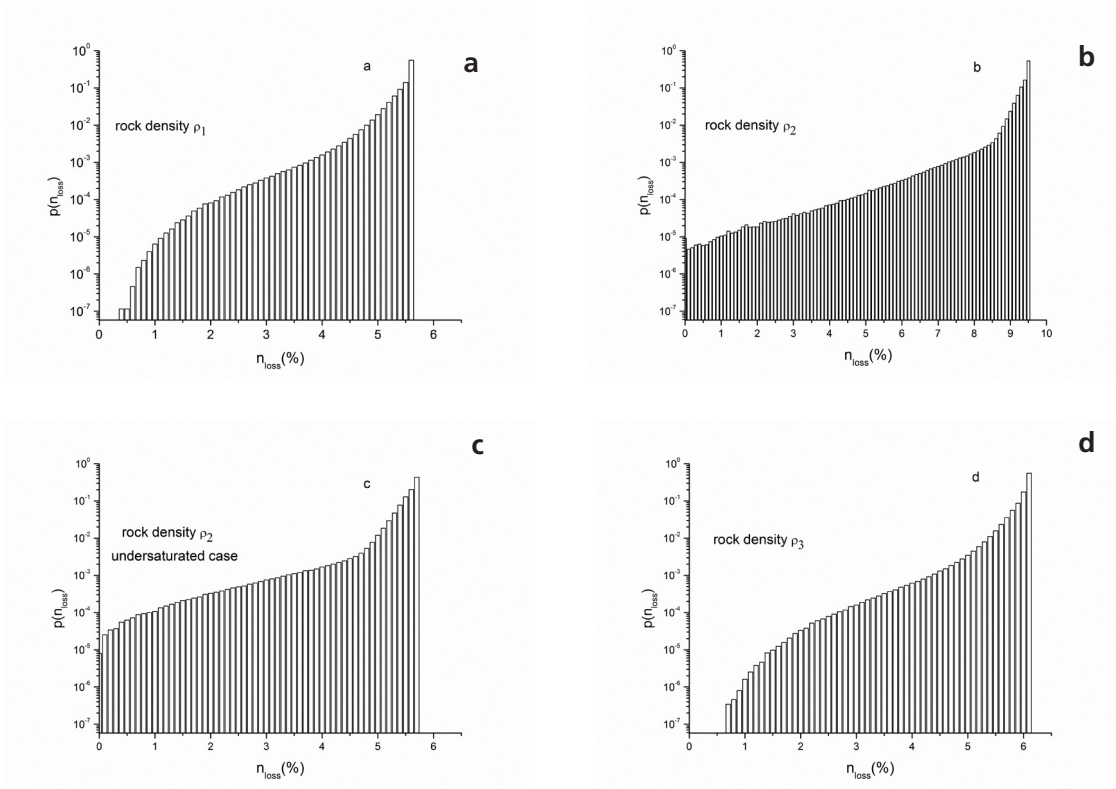
Fig. 4 - Normalized number of eruptions with percentage of gas losses between n_{loss} and $n_{loss}+ \delta$ (with $\delta = 0.1\%$) obtained for a) a constant rock density; b) a density-depth step function; c) a density-depth step function in the undersaturated case; d) a density-depth linear function.
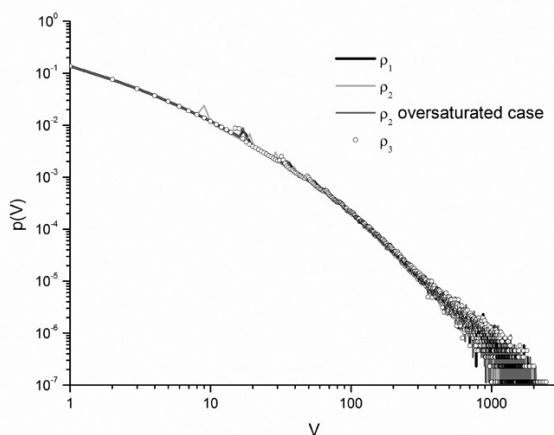
Fig. 5 - Probability of occurrence of an eruptive event as a function of the erupted volume, which is the sum of the values that the field *n* assumes in all fractured cells connected to the surface. The four curves are obtained from the different density-depth functions as in the legend.

$$n_e = n_0 - n_d \tag{3}$$

where n_0 is the initial dissolved water concentration in the magma reservoir.

3. Numerical results

We study the probability of occurrence of a simulated eruptive event, $p(n_{loss})$, with percentage of gas losses between n_{loss} and $n_{loss} + \delta$ (with $\delta = 0.1\%$). We treat statistics of over 10^{10} per run with open boundary conditions, which means that border cells have only three neighbours instead of four. In Fig. 4, we report $p(n_{loss})$ obtained by using the three pressure profiles discussed in the previous section. First of all, we notice that if we approximate the rock density with a step function, $\rho_2(z)$, the number of simulated eruptions (Fig. 4b) shows essentially a linear decreasing behaviour with the percentage of gas loss. Such a linear decreasing behaviour is missing in the other two cases (Figs. 4a and 4d), where the normalized number of eruptions abruptly decreases with lowering of the amount of gas losses. This feature implies that in both cases of constant rock density, ρ_1, and linear rock density, $\rho_3(z)$, eruptions that occur with a very low percentage of gas loss (extreme explosive events) are more unlikely and a minimum threshold value of n_{loss} exists. We observe that the initial dissolved water concentration n_0 (see previous section), which determines the maximum percentage of gas loss of an eruptive event, has similar values in the cases of constant (ρ_1) and linear [$\rho_3(z)$] rock density, where n_0 is about 6%. Instead, by using Eq. (1) when $\rho(z)=\rho_2(z)$, the initial water content dissolved in the liquid results approximately 10% and, therefore, for this case we also study the undersaturated case (Fig. 4c), where the saturation value of the pressure is obtained for $n_0 \cong 6\%$ and gas losses are allowed only at depths for which pressures are less than such a saturation value. Also in the undersaturated case, an essentially linear decrease with the percentage of gas loss is observed, but an increase of the normalized number of eruptions for low gas losses emerges with respect to the saturated case (see

Fig. 4b).

To analyze how the number of eruptions is distributed in terms of erupted volumes, we plot in Fig. 5 the probability of occurrence of an eruption of volume V for the selected density profiles. The volume V is obtained by adding the values of n in all fractured cells connected to the surface. We notice that the size of each cell of our grid is of the order of 10^4 m^3, since we discretize a depth of 12 km (see section 2.3) with 120 square cells and assume a unitary length in the direction orthogonal to the grid. In this way, eruptive events involving from 1 to 1000 cells are characterized by erupted volumes ranging from 10^4 to 10^7 m^3. We specify that the unitless field n quantifies the percentage of magma in a rock cell being $n = 1 - n_e$, where 1 is the value in the magma reservoir and ne depends on the depth as established by Eq. (3). The plot in Fig. 5 shows an approximately linear decrease of the normalized number of eruptions with erupted volumes in a log-log scale, which suggests a characteristic power-law behavior. However, peaks in the probability functions appear in all considered cases. The presence of peaks is explained if we consider that different patterns of fractures filled with magma can provide the same value of V. The more the number of equivalent patterns of fractures is high, the more the peak is pronounced. As it is reasonable to expect, the first peak of $p(V)$ is found when the rock density is approximated by a step function. In this case, the largest number of cells are characterized by the lowest value of the rock density, which causes the largest gas losses and, consequently, the smallest values of V.

4. Conclusions

We studied the effect of three different rock density profiles on the statistical distribution of eruptions in terms of gas losses. We described the magma ascent by means of a field of fractures through which magma can rise (Scandone *et al*., 2007; Piegari *et al*., 2008). The presence of magma in the fractured rock is taken into account by introducing another field, whose values change when degassing processes occur. Since the way of magma degassing depends on the rock density profile, we performed numerical simulation with three rock density profiles to study the effects of such variations on the probability of occurrence of eruptive events. We found that the model gives quite similar results in both the cases of a constant rock density and a rock density linearly dependent on the depth, due to a sort of compensation between the largest and smallest values of the resulting lithostatic pressure. Conversely, if the rock density is approximated by a step function, the normalized number of simulated eruption exhibits an essentially linear decreasing behavior with the percentage of gas loss and extreme events are the most likely to occur, if compared with those predicted by the other two cases. We notice that in this paper we have taken into account only the effects of rock density and have neglected those related to density of magma. Such a simplification is the main limitation of the model, as it does not allow to describe mechanisms of magma buoyancy. For this reason, such a restriction will be relaxed and both the rock and magma densities will be taken into account in future work.

REFERENCES

Bak P.; 1996: *How nature works: the science of self-organized criticality.* Copernicus, New York, NY, USA, 212 pp.

Gardner G.H.F., Gardner L.W. and Gregory A.R.; 1974: *Formation velocity and density – the diagnostic basics for stratigraphic traps*. Geophysics, **39**, 770-780.

Legros F., Kelfoun K. and Martí J.; 2000: *The influence of conduit geometry on the dynamics of caldera-forming eruptions.* Earth Planet. Sci. Lett., **179**, 53-61.

Papale P.; 1999: *Numerical simulations of magma ascent along volcanic conduits.* Phys. Chem. Earth Part A, **24**, 957-961.

Piegari E., Cataudella V., Di Maio R., Milano L. and Nicodemi M.; 2006: *A cellular automaton model for the factor of safety field.* Geophys. Res. Lett., **33**, L01403, doi:10.1029/2005GL024759.

Piegari E., Cataudella V., Di Maio R., Milano L., Nicodemi M. and Scandone R.; 2008: *A model of volcanic magma transport by fracturing stress mechanisms.* Geophys. Res. Lett., **35**, L06308, doi:10.1029/ 2007GL032710.

Piegari E., Di Maio R., Scandone R. and Milano L.; 2011: *A cellular automaton model for magma ascent: degassing and styles of volcanic eruptions.* J. Volcanol. Geotherm. Res., **202**, 22-28, doi:10.1016/ j.jvolgeores.2011.01.007.

Rymer H. and Brown G.C.; 1986: *Gravity fields and the interpretation of volcanic structures: geological discrimination and temporal evolution*. J. Volcanol. Geotherm. Res., **27**, 229-254.

Scandone R. and Giacomelli L.; 1998: *Vulcanologia. Principi fisici e metodi d'indagine.* Liguori, Napoli, Italy, 670 pp.

Scandone R., Cashman K. and Malone S.D.; 2007: *Magma supply, magma ascent and the style of volcanic eruptions.* Earth Planet. Sci. Lett., **253**, 513-529, doi:10.1016/j.epsl.2006.11.016.

Sparks R.S.J.; 1978: *The dynamics of bubble formation and growth in magmas: a review and analysis.* J. Volcanol. Geotherm. Res., **3**, 1-37.

Wilson L. and Head J.W.; 1981: *Ascent and emplacement of basaltic magmas on the Earth and Moon*. J. Geophys. Res., **86**, 2971-3001.

Corresponding author: Ester Piegari
Dipartimento di Scienze della Terra, Università di Napoli "Federico II"
Largo San Marcellino 10, 80138 Napoli, Italy
Phone: +39 081 2538376; fax: +39 081 2538376; e-mail: esterpiegari@g.mail.com